Physica Scripta

Heat transport analysis of aluminum alloy and magnetite graphene oxide through permeable cylinder with heat source/sink

To cite this article before publication: Ramesh G K *et al* 2020 *Phys. Scr.* in press https://doi.org/10.1088/1402-4896/aba5af

Heat transport analysis of aluminum alloy and magnetite graphene oxide through permeable cylinder with heat source/sink

G.K. Ramesh[a], S.A. Shehzad[b], A. Rauf[b], A.J. Chamkha[c,d,*]

[a]Department of Mathematics, K.L.E. Society's J.T. College, Gadag-582101, Karnataka, INDIA

[b]Department of Mathematics, COMSATS University Islamabad, Sahiwal 57000, Pakistan

[c]Institute of Research and Development, Duy Tan University, Da Nang 550000, Vietnam.
[d]Institute of Theoretical and Applied Research (ITAR), Duy Tan University, Hanoi 100000, Vietnam.
[*]Corresponding author email: alichamkha@duytan.edu.vn

Abstract: The flow through a stretchable cylinder has auspicious uses in many industrial processes like thermal processing of food particles, liquid coating on photographic films and tubular heat exchangers. Motivated from these applications, heat transport through a stagnation-point hybrid nanoliquid flow past a permeable cylinder is scrutinized. Aluminum alloy and magnetite graphene oxide with water-based nanoparticles are considered. A uniform heat source/sink term is added in the energy equations. The noted novelty of this work is the application of the hybrid nanofluid along with the heat generation/absorption effect for stretchable cylinders which has not been considered in the open literature. The strong form of ordinary differential coupled equations is solved by the Runge-Kutta-Fehlberg-45 (RKF-45) numerical approach via the shooting technique. Graphical profiles are obtained and discussed at diverse physical parameters. Moreover, the drag friction and the Nusselt number are computed. The results have shown that the higher variation in ϕ_2 causes

a reduction in the velocity and an enhancement in the temperature curves. Further, it is noted that the velocity curves of magnetite graphene oxide is higher than aluminum alloy nanoparticles. The Nusselt number is larger for the aluminum alloy nanoparticles case as compared to the values achieved for the case of magnetite graphene oxide nanoparticles.

Keywords: Aluminum alloy and graphene oxide nanoparticles; Cylinder; heat source/sink; stagnation point; numerical solution.

1. Introduction

The flow phenomenon across a circular cylinder is a topic of fundamental interest among the research community of fluid dynamics. There are various real-life and physical applications usage of such a phenomenon like reduction of drag and vibration, chemical reacting towers, tall buildings chimney stacks at large Reynolds number and compact heat-exchangers at low Reynolds number. Najib et al. [1] discussed mass transport phenomenon in stagnation-point flow subjected to a stretching/shrinking cylinder. It was shown that the curvature parameter modified the shear stresses as well as the mass transfer rate. Moreover, for the shrinking case, dual solutions are appeared while a unique solution is obtained for the stretching cylinder case. Khan et al. [2] inspected the chemical features of flow in a Carreau fluid across a stretching cylinder subjected to homogeneous-heterogeneous reactions. They perceived that the concentration profiles are lower down by the Schmidt number. Shah et al. [3] considered time-dependent viscous fluids flows across a vertical cylinder under thermal memory influence and double stratification. Jogee et al. [4] numerically featured the fluid flow phenomenon through a circular heated cylinder and analyzed a non-linear relation in flow characteristics with temperature beyond 100^{o} C. Gupta et al. [5]

examined thermal and momentum aspects of convective flow induced through power-law fluids under the circular cylinder configuration.

The injection/suction phenomenon through bounding walls has vital interest in engineering applications such as wire coating, coatings of polymer fiber, film cooling, radial diffusers, oil recovery and thrust bearing. The process of injection is valuable in adding reactants, prevent scaling, injection of tissue volume with drug and interstitial space filling. Suction is concerned with chemical processes in order to eliminate reactions and removal of fluids from airways or secretions. Turkyilmazoglu [6] utilized the suction effect to stabilize the asymptotic mean velocity curves owing to a rotating disk. The asymptotic scenario provided a better understanding of flow stabilization. Ishak et al. [7] discussed the suction/blowing and thermal influence on flow outside a circular cylinder. The injection effect was found to lower down the skin friction. Saikrishnan et al. [8] used double slot non-uniform injection (suction) in a laminar flow across a cylinder with fluid properties considered as temperature-dependent functions. Turkyilmazoglu [9] derived analytical expressions of a viscous fluid flow over a rotating disk under the consequences of suction/injection. Khan et al. [10] analyzed the bowing/suction outcomes in flow of a viscous fluid across a nonlinear stretching cylinder using the RKF scheme. Hayat et al. [11] elaborated the injection/suction impacts in a laminar flow subjected to a stretching cylinder and established that the velocity distribution is reduced by larger suction. Bakar et al. [12] investigated suction and stability analysis of steady flow via a stretching/shrinking cylinder through the bvp4c technique. Dual solutions are obtained for a specific range of the suction parameter. The first solution was found to be linearly stable whereas the second one was determined unstable through the stability analysis.

A mixture of homogeneous type that consists of very tiny particles with sizes of 10^{-9} m and a base fluid is termed as nanofluid. Normally, *Cu*, Al_2O_3, *Ag*, *Al* and T_iO_2 are implemented as nanoparticles along base fluids such as ethylene glycol, water and oil. The capability of nano-size particles is of modifying the thermal transport and the thermal conductivity of the working fluid, as metallic particle's specific heat is very much low compared to other liquids or water. A promising significance of nanofluids comprises in nuclear reactors, metallurgical sectors, electronic sectors, power lasers, safer surgery, X-ray generators, lubrication transformation and energy production. Among two different models of nanofluids [13, 14], the Tiwari and Das model [13] assumes solid volume fraction and describes new correlations for the thermal conductivity, thermal diffusivity and heat capacitance of the nanofluid. Sheremet et al. [15] adopted the Tiwari and Das' model in free convective flow through a square cavity with thermal stratification to discuss nanoparticles volume fraction. Das et al. [16] reported the Ag-water and Cu-water nanoparticles flow induced by a convective shrinking surface. They employed the Lie-Group scheme to demonstrate the solutions of problem. Yin et al. [17] analytically examined nanoparticles (*Cu, CuO &* Al_2O_3) attributes in a viscous fluid about a rotating disk. Khan et al. [18] investigated the Falkner-Skan water flow along with nanoparticles (H_2O-aluminm alloy) across a moving wedge. The thermal rate was found to be larger for *AA7075* nanoparticles as compared with *AA7072* nanoparticles. Jyothi et al. [19] analyzed the thermal attributes of a single and multi-wall carbon nanotubes along water through rotating disks having stretching and rotating velocities. Acharya [20] developed a mathematical model to estimate the hydrothermal efficiency by considering the radiative nanoparticles transportation over a bended surface. Doh et al. [21] described nanoparticles (silver) features along water as a base fluid subjected to a variable thickness rotating disk. Silver

nanoparticles volume fraction were found to enhance the tangential and radial flow velocities. Recently, Acharya [22] discussed the solid-liquid interfacial layer and nanoparticles diameter aspects in a ferrofluid flow induced by a spinning disk through an oscillating Lorentz force.

Generally, a nanofluid is famous for enhancing the thermal transport mechanism as a replacement of an ordinary fluid. To advance it in more productive way, the initiative of a hybrid nanofluid is taken. A hybrid nanofluid contains two distinct types of nanoparticles. It is determined that a hybrid nanofluid works in a more effective way than any other ordinary nanofluid. Hybrid nanofluids are convenient in vehicle thermal managing systems, hydro-electric production, spacecraft devices, microelectronics and biomedical production. Devi and Devi [23] described the magnetized hybrid characteristics of Al_2O_3-Cu-water nanoparticles induced by the suction of a permeable moving surface. Ramesh [24] presented heat transport analysis for three distinct hybrid nanoparticles across a rotating disk that saturates the porous medium through the RKF procedure. Ramesh [25] inspected the thermal performance of hybrid nanoparticles (Al_2O_3-Cu/H_2O) in cross and stream wise directions via the RKF scheme. Values of the Nusselt number for platelet shape nanoparticles are more obvious than cylindrical shape nanoparticles. Acharya et al. [26] exhibited the attributes of Hall current in flow of a hybrid nanoliquid (copper/water & titanium dioxide/water) subjected to a spinning disk using the RK-4 technique. They extracted that the Hall parameter can be handy in declining the temperature field. Sheikholeslami et al. [27] dealt with features of a hybrid nanofluid ($MWCNT$-Fe_3O_4/H_2O) confined through circular cavity along with two heaters. The inclusions of hybrid nanoparticles are found to improve thermal transmission. Ramesh et al. [28] analyzed thermochemical responses of hybrid nanoparticles (copper, silver & gold) under the consequences of homogeneous-

heterogeneous reactions and porous medium. They estimated that the hybrid nanofluid temperature can be accelerated through the porosity parameter. Acharya et al. [29,30] addressed the nonlinear radiation and magnetic field features in a hybrid nanofluid flow in a permeable texture and slippery surface. Acharya and Mabood [31] investigated the features of usual and hybrid nanofluids past a slippery bent sheet. They considered the radiative Fe_3O_4-grephene hybrid nanoparticles in this work.

The present study elaborates the thermal performance of hybrid nanoparticles (aluminum alloy and magnetite graphene oxide) with water-based nanoparticles subjected to a permeable circular cylinder. A heat source/sink significance is utilized through the energy equation. The term heat source/sink plays a key role in controlling the thermal performance in situations where a comparatively larger temperature is acquired [32-34]. The impact of suction/injection is also utilized in flow phenomenon. The constitutive flow model is solved with the RKF45 method via the shooting technique. The noted novelty and objective of this work is the application of the hybrid nanofluid theory along with the heat generation/absorption effect for stretchable cylinders which has not been considered in the open literature. This mathematical model has implications in heat exchangers, thermal storage, cooling of micro and electronic chips, hot rolling, paper production and many others.

2. Model and formulation

We are curious to study the flow caused by permeable stretching phenomenon of a cylinder. A hybrid nanoliquid (AA7072-AA7075/H_2O and Fe_3O_4-Go/H_2O) is chosen. Here, it is presumed that the flow is steady, incompressible and two dimensional. Further, the flow is expected in the axial position whereas the radial position is perpendicular to x (see Figure 1). The cylinder has a constant surface temperature

T_w. The stretching velocity and free stream velocity are assumed to vary linearly i.e., $U_w = cx/L, U_e = ax/L$, here c, a are constants and L is the characteristics length. Under these assumptions, the governing two dimensional equations are (Najib et al. [1]):

$$\frac{\partial}{\partial r}(rv)+\frac{\partial}{\partial x}(ru)=0, \tag{1}$$

$$\rho_{hnf}\left(v\frac{\partial u}{\partial r}+u\frac{\partial u}{\partial x}\right)=\mu_{hnf}\left(\frac{1}{r}\frac{\partial u}{\partial r}+\frac{\partial^2 u}{\partial r^2}\right)+U_e\frac{\partial U_e}{\partial x}, \tag{2}$$

$$\left(\rho c_p\right)_{hnf}\left(v\frac{\partial T}{\partial r}+u\frac{\partial T}{\partial x}\right)=k_{hnf}\left(\frac{1}{r}\frac{\partial T}{\partial r}+\frac{\partial^2 T}{\partial r^2}\right)+Q_0(T-T_\infty), \tag{3}$$

The boundary conditions for the designed problem are:

$$\begin{aligned} &v=V_w, u=U_w, T=T_w \text{ at } r=R, \\ &u\to U_e, T\to T_\infty \text{ as } r\to\infty. \end{aligned} \tag{4}$$

Here, v and u refer to the velocity components in the r and x movement, T is the hybrid nanoliquid temperature, Q_0 is the uniform heat sink and source, ρ_{hnf} is the density of the hybrid nanoliquid, μ_{hnf} is the viscosity of the hybrid nanoliquid, $(\rho c_p)_{hnf}$ is the heat capacitance of the hybrid nanoliquid and k_{hnf} is the thermal conductance of the hybrid nanoliquid.

The thermo-physical properties of the hybrid nanoliquid are (see Devi and Devi [23]):

$$\rho_{hnf} = \phi_2\rho_{s2} + (1-\phi_2)\left[\rho_{s1}\phi_1 + (1-\phi_1)\rho_f\right], \mu_{hnf} = \frac{\mu_f}{(1-\phi_1)^{2.5}(1-\phi_2)^{2.5}},$$

$$\left(\rho c_p\right)_{hnf} = \left(\rho c_p\right)_{s2}\phi_2 + (1-\phi_2)\left[\phi_1\left(\rho c_p\right)_{s1} + \left(\rho c_p\right)_f(1-\phi_1)\right],$$

$$k_{hnf} = \frac{k_{bf}(n-1) + k_{s_2} - \phi_2(k_{bf} - k_{s_2})(n-1)}{\phi_2(k_{bf} - k_{s_2}) + k_{s_2} + k_{bf}(n-1)}k_{bf},$$

where $k_{bf} = \dfrac{(n-1)k_f + k_{s_1} + \phi_1(k_{s_1} - k_f)(n-1)}{(n-1)k_f + k_{s_1} - \phi_1(k_{s_1} - k_f)}k_f.$

Here ϕ_1, ϕ_2 are the volume fraction of hybrid nanoparticles, f, nf, hnf, s_1, s_2 demonstrate the fluid, nanofluid, hybrid-nanofluid, solid nanoparticles, respectively and $n = 3$ corresponds to spherical shaped nanoparticles.

Taking the desirable transformations as (Najib et al. [1])

$$\psi = \left(\frac{\nu_f a}{L}\right)^{1/2} x\,\mathrm{R}\, f(\zeta),\ \zeta = \frac{r^2 - R^2}{2R}\left(\frac{a}{\nu_f L}\right)^{1/2}, \theta(\zeta) = \frac{T - T_\infty}{T_w - T_\infty}, \tag{5}$$

By substituting (5) into (1) - (4), one can obtain the following form of the equations:

$$\frac{[(1+2\zeta K)f''' + 2Kf'']}{(1-\phi_1)^{2.5}(1-\phi_2)^{2.5}\left\{(1-\phi_2)\left[(1-\phi_1) + \phi_1\left(\frac{\rho_{s_1}}{\rho_f}\right)\right] + \phi_2\left(\frac{\rho_{s_2}}{\rho_f}\right)\right\}} + ff'' - f'^2 + 1 = 0 \tag{6}$$

$$\left(\frac{k_{hnf}}{k_f}\right)\frac{[(1+2\zeta K)\theta'' + 2K\theta']}{(1-\phi_2)\left[(1-\phi_1) + \phi_1\dfrac{(\rho c_p)_{s_1}}{(\rho c_p)_f}\right] + \phi_2\dfrac{(\rho c_p)_{s_2}}{(\rho c_p)_f}} + \mathrm{Pr}(f\theta' - f'\theta) + Q\theta = 0 \tag{7}$$

with

$$\begin{aligned} &f = S, f' = \varepsilon, \theta = 1 \text{ at } \zeta = 0, \\ &f' \to 1, \theta \to 0 \text{ as } \zeta \to \infty, \end{aligned} \tag{8}$$

From equations (6) to (8), the following physical parameters are obtained

$K = \left(\frac{\nu_f L}{aR^2}\right)^{1/2}$ for curvature parameter,

$\varepsilon = \frac{c}{a}$ for velocity ratio parameter,

$S = -\frac{V_w r}{R}\left(\frac{L}{\nu_f a}\right)^{1/2}$ for suction/injection parameter

$Q = \frac{Q_o L}{a(\rho c_p)_f}$ for heat source/sink parameter

$\Pr = \frac{\mu_f \left(c_p\right)_f}{k_f}$ for Prandtl number

The intention of this model is to find the variation of the drag friction which is directly proportional to $-f''(0)$ and the Nusselt number which is directly proportional to $-\theta'(0)$ for different physical parameter which are presented in the problem.

The expression of the drag friction and the Nusselt number is defined as

$$C_f = \frac{\tau_w}{U_w^2 \rho_f},\ Nu = \frac{x q_w}{k_f (T_w - T_\infty)}, \tag{9}$$

Here τ_w and q_w are the shear stress and the heat flux at the surface which are presented as

$$\tau_w = \mu_{hnf}\left(\frac{\partial u}{\partial r}\right)_{r=R}, q_w = -k_{hnf}\left(\frac{\partial T}{\partial r}\right)_{r=R}. \tag{10}$$

By exploitation of (5), one can have

$$C_f \,\mathrm{Re}_x^{1/2} = \frac{f''(0)}{(1-\phi_1)^{2.5}(1-\phi_2)^{2.5}}, Nu\,\mathrm{Re}_x^{-1/2} = -\frac{k_{hnf}}{k_f}\theta'(0), \tag{11}$$

where $\mathrm{Re}_x = \dfrac{U_w x}{\nu_f}$ is the local Reynolds number.

Computational Method

The solution of the problem is obtained by converting equations (6) to (8) into first-order ordinary differential equations

$$f_1 = f',\ f_2 = f_1',\ f_3 = \theta',$$

$$\frac{[(1+2\zeta K) f_2' + 2K f_2]}{(1-\phi_1)^{2.5}(1-\phi_2)^{2.5}\left\{(1-\phi_2)\left[(1-\phi_1)+\phi_1\left(\frac{\rho_{s_1}}{\rho_f}\right)\right]+\phi_2\left(\frac{\rho_{s_2}}{\rho_f}\right)\right\}} + f f_2 - f_1^2 + 1 = 0,$$

$$\left(\frac{k_{hnf}}{k_f}\right)\frac{[(1+2\zeta K) f_3' + 2K f_3]}{(1-\phi_2)\left[(1-\phi_1)+\phi_1\dfrac{(\rho c_p)_{s_1}}{(\rho c_p)_f}\right]+\phi_2\dfrac{(\rho c_p)_{s_2}}{(\rho c_p)_f}} + \mathrm{Pr}(f f_3 - f_1\theta) + Q\theta = 0,$$

$$f(0) = S,\ f_1(0) = \varepsilon, \theta(0) = 1,\ f_1(\infty) = 1, \theta(\infty) = 0.$$

The algorithm program of the Runge-Kutta- Fehlberg –forth- fifth order method is given by;

Runge-Kutta method of order 4:

$$y_{i+1} = y_i + \frac{25}{216}k_1 + \frac{1408}{2565}k_3 + \frac{2197}{4104}k_4 - \frac{1}{5}k_5$$

Runge-Kutta method of order 5:

$$z_{i+1} = y_i + \frac{16}{135}k_1 + \frac{6656}{12{,}825}k_3 + \frac{28{,}561}{56{,}430}k_4 - \frac{9}{50}k_5 + \frac{2}{55}k_6$$

and 6 steps size as follows

$$k_1 = hf(x_i, y_i)$$
$$k_2 = hf(x_i + \frac{1}{4}h, y_i + \frac{1}{4}k_1)$$
$$k_3 = hf(x_i + \frac{3}{8}h, y_i + \frac{3}{32}k_1 + \frac{9}{32}k_2)$$
$$k_4 = hf(x_i + \frac{12}{13}h, y_i + \frac{1932}{2197}k_1 - \frac{7200}{2197}k_2 + \frac{7296}{2197}k_3)$$
$$k_5 = hf(x_i + h, y_i + \frac{439}{216}k_1 - 8k_2 + \frac{3680}{513}k_3 - \frac{845}{4104}k_4)$$
$$k_6 = hf(x_i + \frac{1}{2}h, y_i - \frac{8}{27}k_1 + 2k_2 - \frac{3544}{2565}k_3 - \frac{1859}{4104}k_4 - \frac{11}{40}k_5)$$

The above set of equations are solved using the RKF-45 method by executing the missing values through the shooting approach. For this, we adopted h = 0.1, tolerance = 10^{-6} and $\varepsilon = 2, K = 0.5, S = 0.5, Q = 0.5, \phi_1 = 0.1$ and Pr = 6.2. The thermo-physical properties of different nanoparticles and water are given in Table 1.

3. Results and discussion

The current section presents the numerical values and graphical results of the derived physical quantities such as $K, \varepsilon, S, Q, \Pr, \phi_2$ and nanoparticles. Table 1 presents the nanoparticles and water thermos-physical characteristics as studied by [15, 18]. Table 2 is drawn to show the validity of the numerical procedure for the drag friction with the literature work [1] for the limiting scenario, that is, $\phi_1 = \phi_2 = S = Q = 0, \varepsilon = -0.25$ and $K = 0.2, 0.4$. Excellent comparison for $f''(0)$ is observed. Table 3 illustrates the drag friction and the thermal rate of hybrid nanoparticles for increased values of ε, K, S, Q and ϕ_2. The magnitude of the drag friction for *AA7072-AA7075/H_2O and Fe_3O_4-Go/H_2O* is increased against enhanced ε, K, S and ϕ_2 values. The magnitude of the heat transfer rate of the hybrid nanoparticles become larger for the modified velocity ratio, curvature and the suction/injection parameters values, while against the

heat source/sink parameter and the volume fraction of hybrid nanoparticles such a thermal rate has a reducing tendency.

The demonstration of the velocity curves for hybrid nanoparticles can be viewed through Fig. 2. Fig. 3 explains the hybrid nanoparticles thermal features. From Figs. 2 and 3, it is observed that the behavior of the velocity and thermal curves for nanoparticles is quite the opposite. Moreover, the temperature curves are very close to each other as compared with the velocity curves for distinct nanoparticles. Figs. 4 and 5 explain the curvature parameter impact on f' and θ for two different hybrid nanoparticles. The velocity profiles in Fig. 4 illustrate the increasing tendency against the curvature parameter $(K = 0.5, 2, 2.5)$. However, the velocity curves of magnetite grapheme oxide nanoparticles are larger than those for the aluminum alloy. The velocity is enhanced by increasing the curvature constraint values. From a physical aspect, the lower kinematic viscous factor appears for larger values of the curvature parameter due to which the liquid moves freely which enhances the velocity profile. The curvature parameter outcomes on the thermal curves are sketched via Fig. 5. The temperature field is also showing an increasing trend against the enhanced values of K. It is also perceived that nanoparticles *AA7072-AA7075/H_2O* and *Fe_3O_4-Go/H_2O* have almost a similar kind of influence on the thermal field (see Fig. 5). The suction/injection parameter impacts on the velocity and temperature fields are elaborated by Figs. 6 and 7. Both the velocity and temperature curves correspond to nanoparticles increase with imposed suction and decrease with respect to imposed injection. The velocity at the wall is enhanced for increasing the suction parameter and lesser for incrementing the injection parameter. The larger wall velocity improves the velocity of a flowing material due to which a higher velocity field is obtained in the case of an increasing suction parameter. In fact, the liquid leaves the system faster in the case of an increasing

suction parameter due to which the velocity of liquid in the system is enhanced. Further, in the injection case, more liquid enters into the system which reduces the velocity of material. The velocity curves of *Fe_3O_4-Go/H_2O* are larger from those for *AA7072-AA7075/H_2O* for the suction case, while in case of injection, the scenario is quite the opposite. From Fig. 7, it is obvious that nanoparticles have a similar kind of impact on the temperature curves with respect to S. Figs. 8 and 9 delineate the consequences of ε on the velocity as well as the temperature fields, respectively. The velocity ratio parameter has a significant influence on f' by considering *AA7072-AA7075/H_2O* and *Fe_3O_4-Go/H_2O*. Increasing the value of ε tends to accelerate the flow field; therefore the curves f' depict an enhancing nature. The velocity curves against the magnetite grapheme oxide nanoparticles are greater than the velocity curves of aluminum alloy nanoparticles (see Fig. 8). In Fig. 9, the temperature field also exhibits an increasing phenomenon for ε, however, there is less amount of difference noticed against the thermal curves of the nanoparticles under consideration. Fig. 10 is pictured in order to signify the influence of the heat source/sink parameter on θ. For $Q > 0$ (heat source), the increasing trend in the temperature curves is established, however, the phenomenon is quite the reverse for $Q < 0$ (heat sink). The nanoparticles have a similar influence on θ compared to each other. The larger heat source constraint implies more heat in the system which enhances the temperature. For larger values of heat sink, the energy will be lost due to which a lower temperature field is observed.

Figs. 11 and 12 are designed to describe the impact of the volume fraction of hybrid nanoparticles on f' and θ. The velocity curves are reduced, while the temperature profiles are enhanced by increasing the variation in ϕ_2. The velocity curves of *AA7072-AA7075/H_2O* are larger in this case from those corresponding to *Fe_3O_4-Go/H_2O*.

Moreover, magnetite grapheme oxide nanoparticles have a more significant impact on the velocity field than that of the aluminum alloy. The impact of ϕ_2 corresponds to hybrid nanoparticles is not significant on θ and can be observed from Fig. 12. The volume fraction of hybrid nanoparticles and the velocity ratio parameter impacts on heat transfer rate for magnetite grapheme oxide and aluminum alloy nanoparticles are described in Fig. 13. The heat transfer rate of *AA7072-AA7075*/water is found to be larger than that for *Fe_3O_4-Go/*water. Furthermore, for increased values of ϕ_2 and ε, the thermal rate is reduced (see Fig. 13). Fig. 14 presents the behavior of the Nusselt number against different Q and ε values. The Nusselt number depicts a decreasing trend for increased values of Q and ε corresponding to hybrid nanoparticles. Figs. 15 and 16 are sketched to draw the streamlines pattern for *AA7072-AA7075/H_2O* and *Fe_3O_4-Go/H_2O*, respectively. A similar behavior of the streamlines are observed from Figs. 15 and 16 against nanoparticles *AA7072-AA7075/H_2O* and *Fe_3O_4-Go/H_2O*.

4. Final remarks

In the present work, energy transportation in stagnation-point hybrid nanomaterials flow past a permeable cylinder is demonstrated. The mixture of aluminum alloy and magnetite graphene oxide in water is accounted as a working fluid. The numerical methodology is developed to express the pictorial and tabular results of the problem. The key results of this research are listed as follows:

- The drag coefficient $f''(0)$ and Nusselt number $\theta'(0)$ values against incrementing values of physical constraints are larger for *AA7072-AA7075/H_2O* nanoparticles as compared to the values achieved in the case of *Fe_3O_4-Go/H_2O* nanoparticles consideration.

- The velocity for a hybrid nanofluid is higher than that for a regular nanoliquid for incrementing values of the curvature parameter.
- The higher curvature constraint improves the temperature θ. The temperature of a hybrid nanofluid is higher compared to the usual nanoliquid for enhancing values of the curvature constraint.
- The temperature is boosted in the case of a heat source $(Q > 0)$ and is decayed for a heat sink $(Q < 0)$ situation.
- The temperature is enhanced by enhancing the values of the suction/injection parameter. The suction/injection phenomenon is encountered in the petroleum industry and under-ground water resources.
- The temperature of *Fe_3O_4-Go/water* type nanofluid is higher compared to the temperature of *A7072-AA7075/water*, *AA7075/water* and *Fe_3O_4 /water* types nanofluids.
- The improvement in nanoparticles volume fraction values results in weaker velocity and higher temperature profiles.
- The temperature $\boldsymbol{\theta}$ of hybrid nanofluids is higher than the temperature of ordinary nanofluids.

Conflict of Interest: The authors declare that they have no conflict of interest.

Acknowledgement: The authors are very much thankful to the editor and the referees for their encouraging comments and constructive suggestions to improve the presentation of this manuscript.

References

[1] N. Najib, N. Bachok, N. M. Arifin and A. Ishak, Stagnation point flow and mass transfer with chemical reaction past a stretching/shrinking cylinder, Scientific Reports, 4, 2014, 4178.

[2] I. Khan, S. Ullah, M. Y. Malik and A. Hussain, Numerical analysis of MHD Carreau fluid flow over a stretching cylinder with homogeneous-heterogeneous reactions, Results in Physics, 9, 2018, 1141-1147.

[3] N. A. Shah, N. Ahmed, D. Vieru and C. Fetecau, Effects of double stratification and heat flux damping on convective flows over a vertical cylinder, Chinese Journal of Physics, 60, 2019, 290-306.

[4] S. Jogee, B. V. S. S. S. Prasad and K. Anupindi, Large-eddy simulation non-isothermal flow over a circular cylinder, International Journal of Heat and Mass Transfer, 151, 2020, 119426.

[5] S. Gupta, S. A. Patel and R. P. Chhabra, Pulsatile flow of power-law fluids over a heated cylinder: Flow and heat transfer characteristics, International Journal of Thermal Sciences, 152, 2020, 106330.

[6] M. Turkyilmazoglu, An asymptotic investigation into the stabilization effect of suction in the rotating-disk boundary layer flow, Computers & Mathematics with Applications, 53, 2007, 750-759.

[7] A. Ishak, R. Nazar and I. Pop, Uniform suction/blowing effect on flow and heat transfer due to a stretching cylinder, Applied Mathematical Modelling, 32, 2008, 2059-2066.

[8] P. Saikrishnan, S. Roy, I. M. R. Sadiq and B. D. Pandey, Non-uniform double slot suction (injection) into water boundary layer flows over a cylinder, International Journal of Heat and Mass Transfer, 52, 2009, 894-898.

[9] M. Turkyilmazoglu, Analytic approximate solutions of rotating disk boundary layer flow subject to a uniform suction or injection, International Journal of Mechanical Sciences, 52, 2010, 1735-1744.

[10] M. I. Khan, M. Tamoor, T. Hayat and A. Alsaedi, MHD boundary layer thermal slip flow by nonlinearly stretching cylinder with suction/blowing and radiation, Results in Physics, 7, 2017, 1207-1211.

[11] T. Hayat, M. I. Khan, M. Waqas and A. Alsaedi, Newtonian heating effect in nanofluid by a permeable cylinder, Results in Physics, 7, 2017, 256-262.

[12] N. A. A. Bakar, N. Bachok, N. M. Arifin and I. Pop, Stability analysis on the flow and heat transfer of nanofluid past a stretching/shrinking cylinder with suction effect, Results in Physics, 9, 2018, 1335-1344.

[13] J. Buongiorno, Convective transport in nanofluids, Journal of Heat Transfer, 128, 2006, 240-250.

[14] R. K. Tiwari and M. K. Das, Heat transfer augmentation in a two-sided lid-driven differentially heated square cavity utilizing nanofluids, International Journal of Heat and Mass Transfer, 50, 2007, 2002-2018.

[15] M. A. Sheremet, S. Dinarvand and I. Pop, Effect of thermal stratification on free convection in a square porous cavity filled with a nanofluid Tiwari and Das' nanofluid model, Physica E: Low-dimensional Systems and Nanostructures, 69, 2015, 332-341.

[16] K. Das, N. Acharya and P.K. Kundu, The onset of nanofluid flow past a convectively heated shrinking sheet in presence of heat source/sink: A Lie group approach, Applied Thermal Engineering, 103, 38-46 (2016).

[17] C. Yin, L. Zheng, C. Zhang and X. Zhang, Flow and heat transfer of nanofluids over a rotating disk with uniform stretching rate in radial direction, Propulsion and Power Research, 6, 2017, 25-30.

[18] U. Khan, Adnan, N. Ahmed and S. T. Mohyud-Din, Heat transfer enhancement in hydromagnetic dissipative flow past a moving wedge suspended by H_2O-aluminum

alloy nanoparticles in the presence of thermal radiation, International Journal of Hydrogen Energy, 42, 2017, 24634-24644.

[19] K. Jyothi, P. S. Reddy and M. S. Reddy, Influence of magnetic field and thermal radiation on convective flow on SWCNTs-water and MWCNTSs-water nanofluid between rotating stretchable disks with convective boundary condition, Powder Technology, 331, 2018, 326-337.

[20] N. Acharya, Spectral quasi linearization simulation of radiative nanofluidic transport over a bended surface considering the effects of multiple convective conditions, European Journal of Mechanics-B/Fluids, 84, 139-154 (2020).

[21] D. Doh, M. Muthtamilselvan, B. Swathene and E. Ramya, Homogeneous and heterogeneous reactions in a nanofluid flow due to a rotating disk of variable thickness using HAM, Mathematics and Computers in Simulation, 168, 2020, 90-110.

[22] N. Acharya, Framing the impacts of highly oscillating magnetic field on the ferrofluid flow over a spinning disk considering nanoparticle diameter and solid liquid interfacial layer, Journal of Heat Transfer (2020) https://doi.org/10.1115/1.4047503.

[23] P.A. Devi, S.S.U. Devi, Numerical investigation of hydromagnetic hybrid *Cu*-Al_2O_3/water nanofluid flow over a permeable stretching sheet with suction, International Journal of Nonlinear Sciences and Numerical Simulation 17 (2016) 249-257.

[24] G. K. Ramesh, Three different hybrid nanomaterial performances on rotating disk: A non-Darcy model, Applied Nanoscience, 9, 2019, 179-187.

[25] G. K. Ramesh, Influence of shape factor on hybrid nanomaterial in a cross flow direction with viscous dissipation, Physica Scripta, 94, 2019, 105224.

[26] N. Acharya, R. Bag and P. K. Kundu, Influence of Hall current on radiative nanofluid flow over a spinning disk: A hybrid approach, Physica E: Low-dimensional Systems and Nanostructures, 111, 2019, 103-112.

[27] M. Sheikholeslami, S. A. M. Mehryan, A. Shafee and M. A. Sheremet, Variable magnetic forces impact on magnetizable hybrid nanofluid heat transfer through a circular cavity, Journal of Molecular Liquids, 277, 2019, 388-396.

[28] G.K. Ramesh, S. Manjunatha and B.J. Gireesha, Impact of homogeneous-heterogeneous reactions in a hybrid nanoliquid flow due to porous medium, Heat Transfer Asian Research, 48, 2019, 3866-3884.

[29] N. Acharya, R. Bag and P.K. Kundu , On the impact of nonlinear thermal radiation on magnetized hybrid condensed nanofluid flow over a permeable texture, Applied Nanoscience, 10, 1679-1691 (2020).

[30] N. Acharya, S. Maity and P.K. Kundu, Influence of inclined magnetic field on the flow of condensed nanomaterial over a slippery surface: the hybrid visualization, Applied Nanoscience, 10, 633-647 (2020).

[31] N. Acharya and F. Mabood, On the hydrothermal features of radiative Fe_3O_4-graphene hybrid nanofluid flow over a slippery bended surface with heat source/sink, Journal of Thermal Analysis and Calorimetry (2020) https://doi.org/10.1007/s10973-020-09850-1

[32] A. Rauf, Z. Abbas and S. A. Shehzad, Chemically reactive hydromagnetic flow over a stretchable oscillatory rotating disk with thermal radiation and heat source/sink: A numerical study, Heat Transfer Research, 50, 2019, 1495-1512.

[33] G. K. Ramesh, K. G. Kumar, B. J. Gireesha, S. A. Shehzad and F. M. Abbasi, Magnetohydrodynamic nanoliquid due to unsteady contracting cylinder with uniform

heat generation/absorption and convective condition, Alexandria Engineering Journal, 57, 2018, 3333-3340.

[34] J. Ahmad, M. Khan and L. Ahmad, Stagnation point flow of Maxwell nanofluid over a permeable rotating disk with heat source/sink, Journal of Molecular Liquids, 287, 2019, 110853.

Table 1: Thermo-Physical properties of nano-particles and water (Sheremet et al. [15] and Khan et al. [17])

Particles	$\rho(kg/m^3)$	$c_p(J/kg\,K)$	$k(W/mk)$
*AA*7072	2720	893	222
*AA*7075	2810	960	173
Fe_3O_4	5180	670	9.7
Go	1800	717	5000
Water	997.1	4179	0.613

Table 2: Comparison of the values of $f''(0)$ for different values of ε and K when $\phi_1 = \phi_2 = S = Q = 0$.

	Najib et al. [1]		Comparison study	
ε	$K = 0.2$	$K = 0.4$	$K = 0.2$	$K = 0.4$
-0.25	1.5396153	1.6672783	1.5396512	1.6675985

Table 3: Computational values of $f''(0)$ and $\theta'(0)$ for different physical parameters.

					AA7072-AA7075/H_2O		Fe_3O_4-Go/H_2O	
ε	K	S	Q	ϕ_2	$-f''(0)$	$-\theta'(0)$	$-f''(0)$	$-\theta'(0)$
1.2	0.5	0.5	0.5	0.01	0.4098184	4.046329	0.396397	3.968089
1.5					1.064344	4.330551	1.029519	4.249760
2					2.253774	4.758861	2.180121	4.673905
2	0.5	0.5	0.5	0.01	2.253774	4.758861	2.180121	4.673905
	2				2.829836	5.268760	2.754633	5.184959
	2.5				3.007563	5.436179	2.931705	5.352567
2	0.5	-0.5	0.5	0.01	1.784960	2.291543	1.741115	2.277384

		0.0			2.008173	3.374559	1.950520	3.331833
		0.5			2.253774	4.758861	2.180121	4.673905
2	0.5	0.5	-0.5	0.01	2.253774	5.343307	2.180121	5.250185
			0.0		2.253774	5.062300	2.180121	4.973116
			0.5		2.253774	4.758861	2.180121	4.673905
2	0.5	0.5	0.5	0.01	2.253774	4.758861	2.180121	4.673905
				0.02	2.239374	4.656518	2.191939	4.598363
				0.03	2.224604	4.557539	2.202139	4.524836

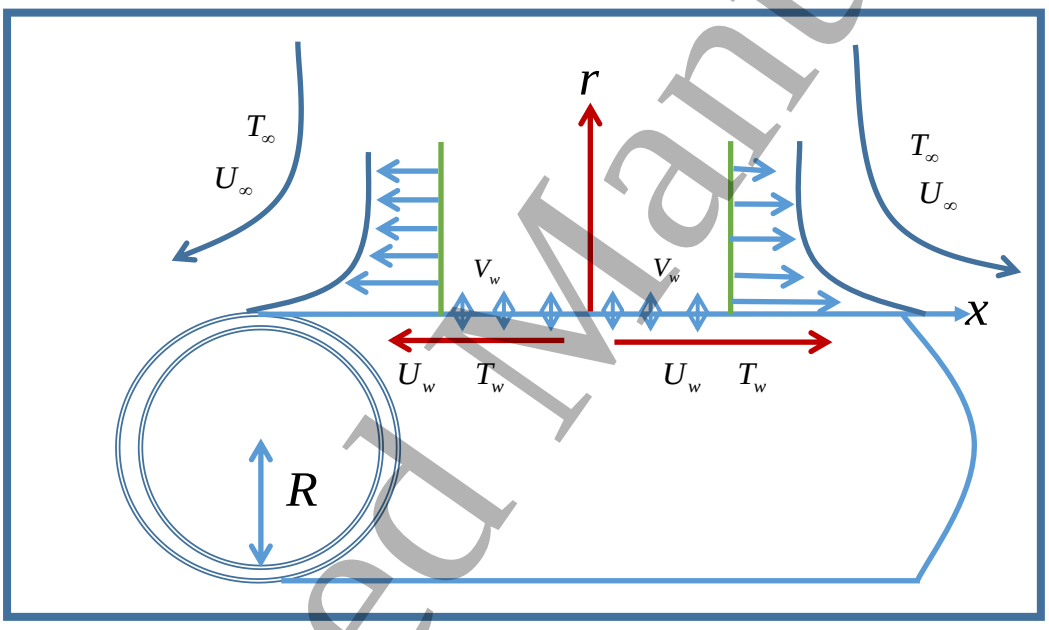

Fig. 1: Geometry of the problem.

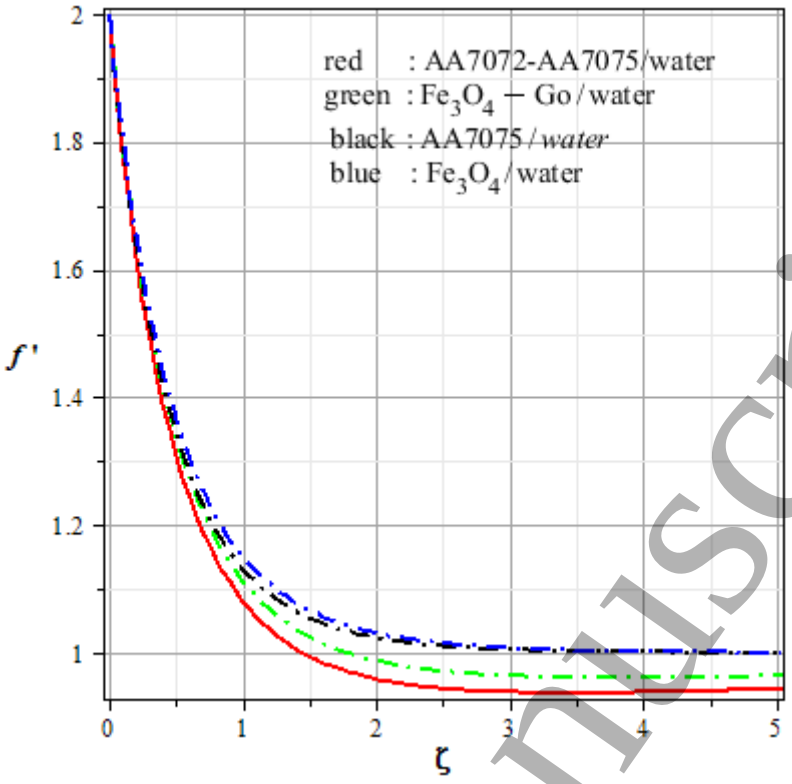

Fig. 2: Velocity curve for different nanoparticles.

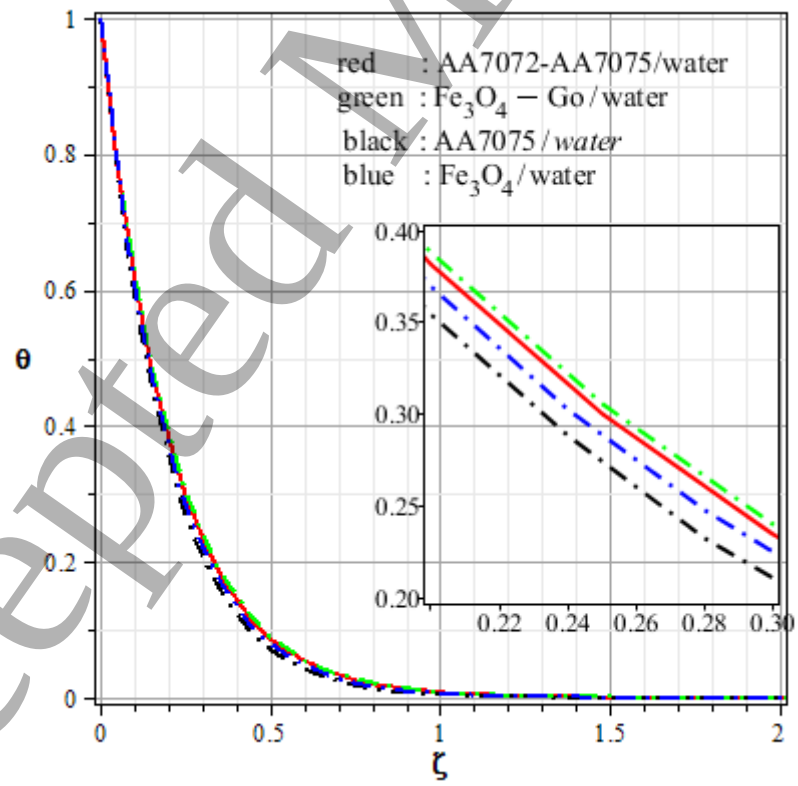

Fig. 3: Temperature curve for different nanoparticles.

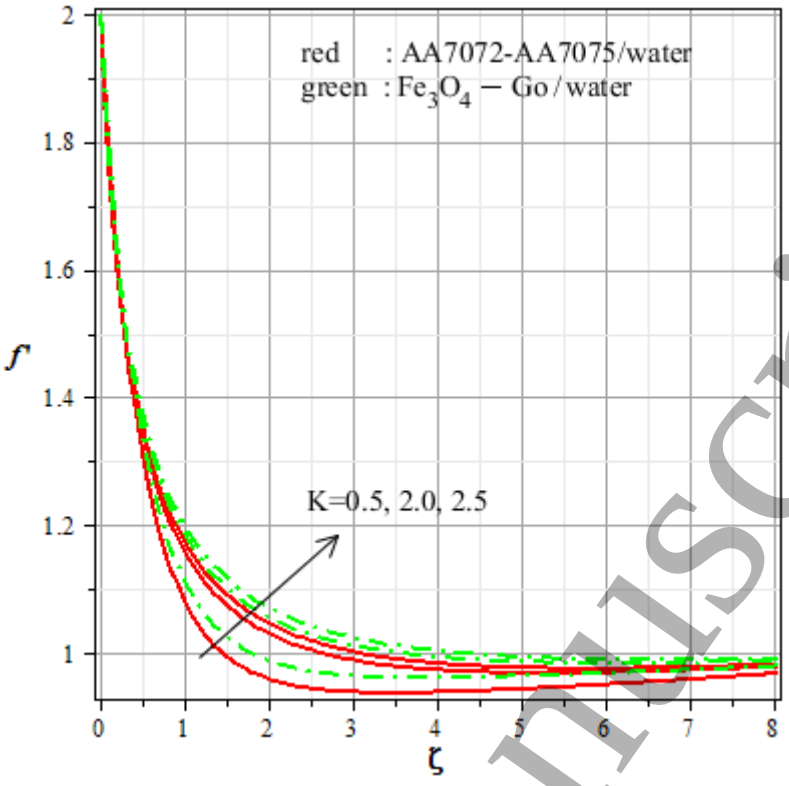

Fig. 4: Velocity curve for different K.

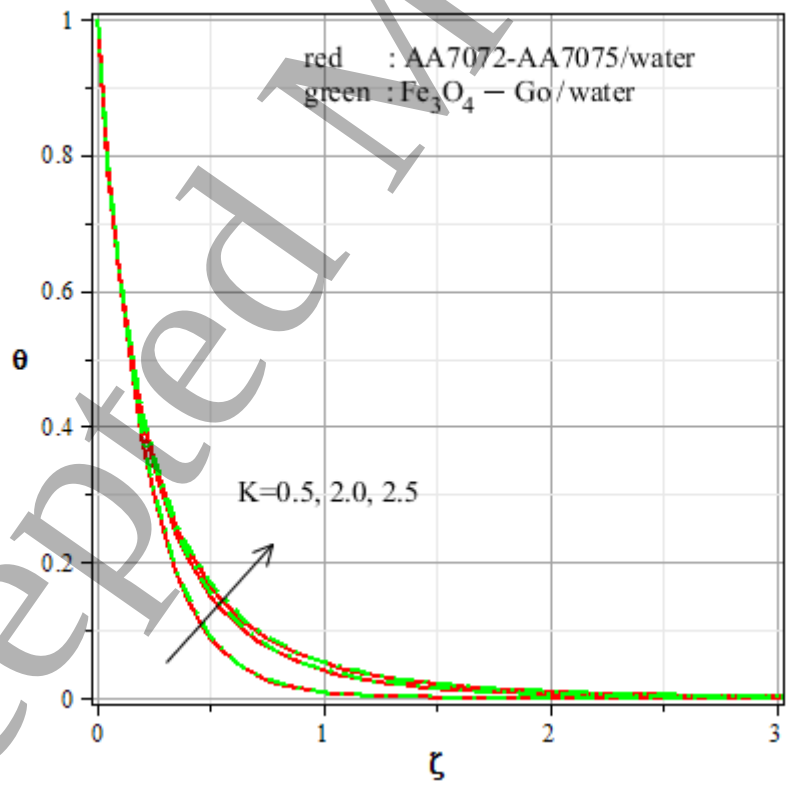

Fig. 5: Temperature curve for different K.

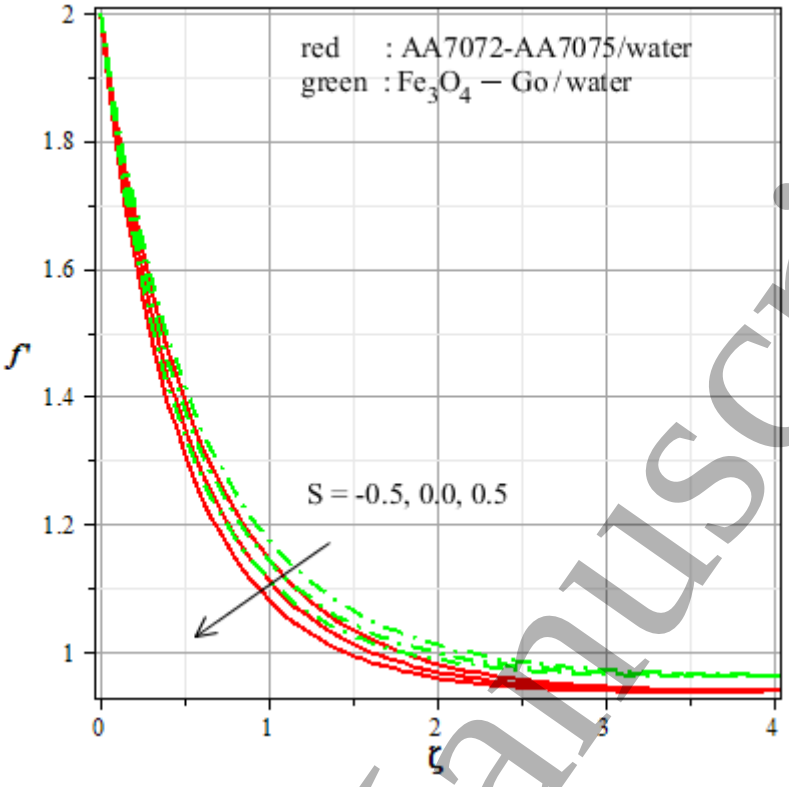

Fig. 6: Velocity curve for different S.

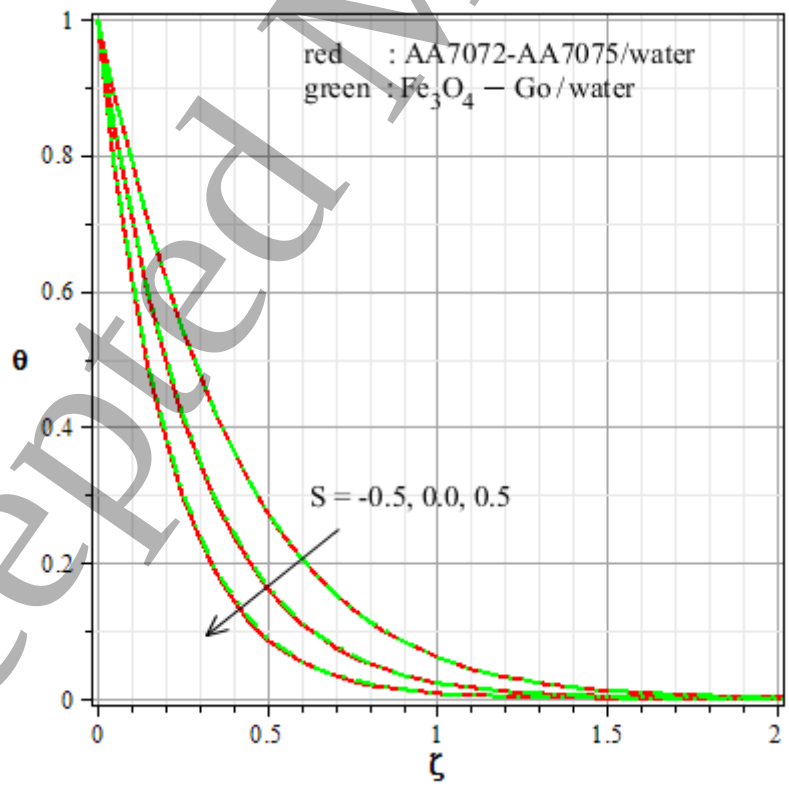

Fig. 7: Temperature curve for different S.

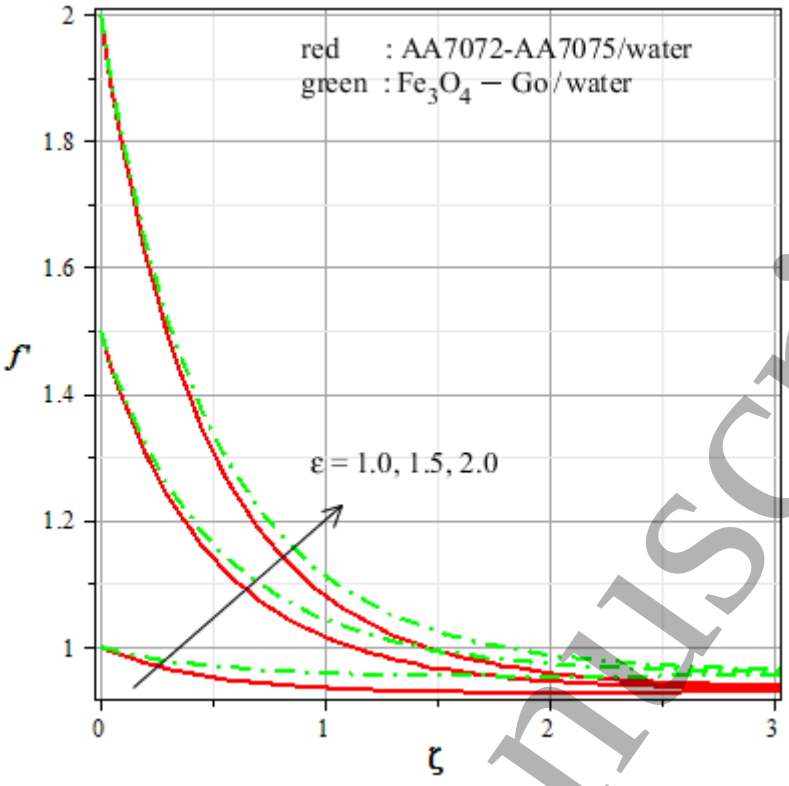

Fig. 8: Velocity curve for different ε.

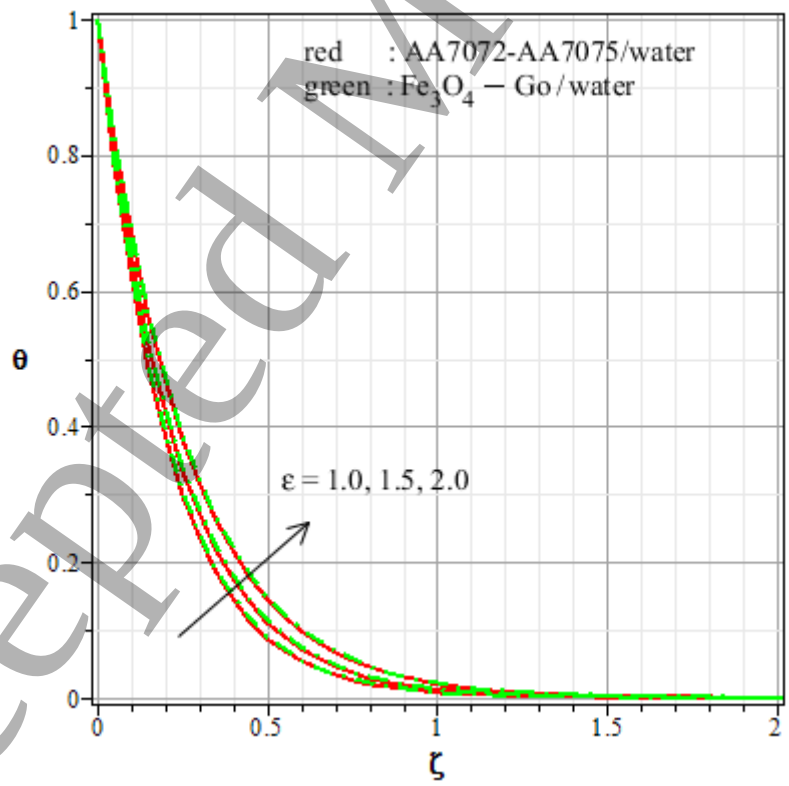

Fig. 9: Temperature curve for different ε.

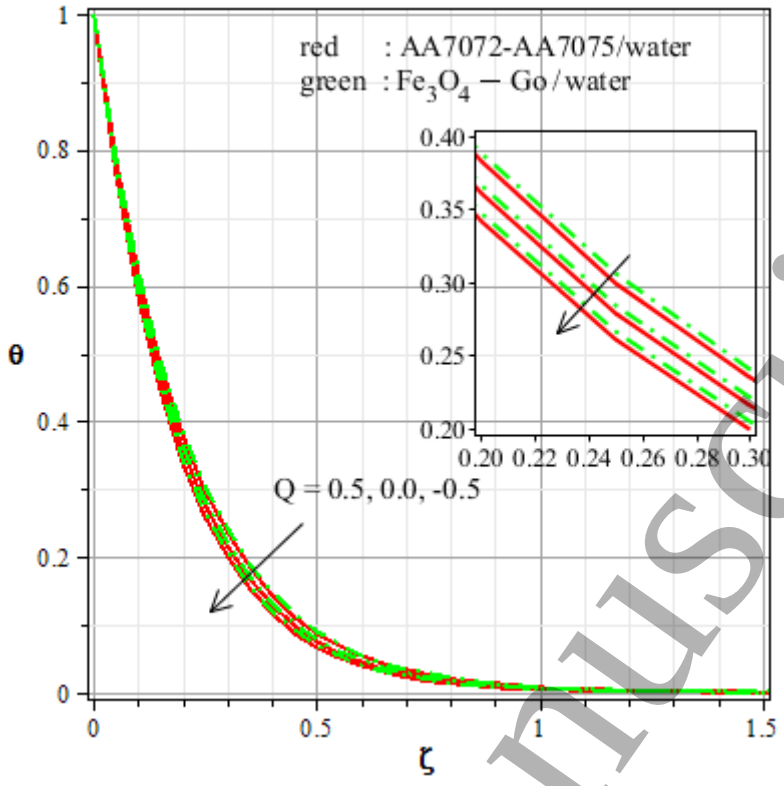

Fig. 10: Temperature curve for different Q.

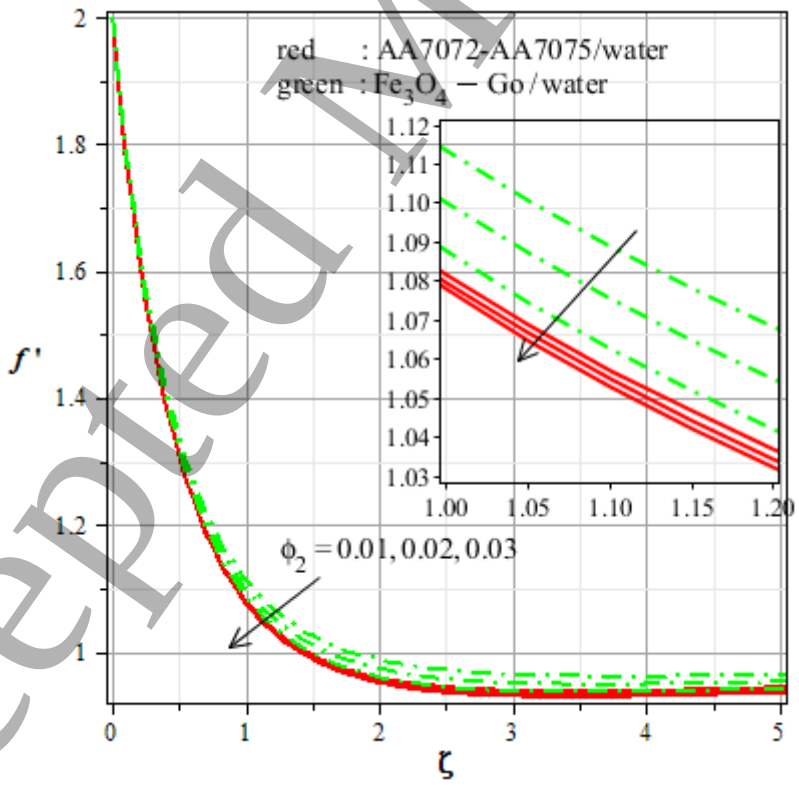

Fig. 11: Velocity curve for different ϕ_2.

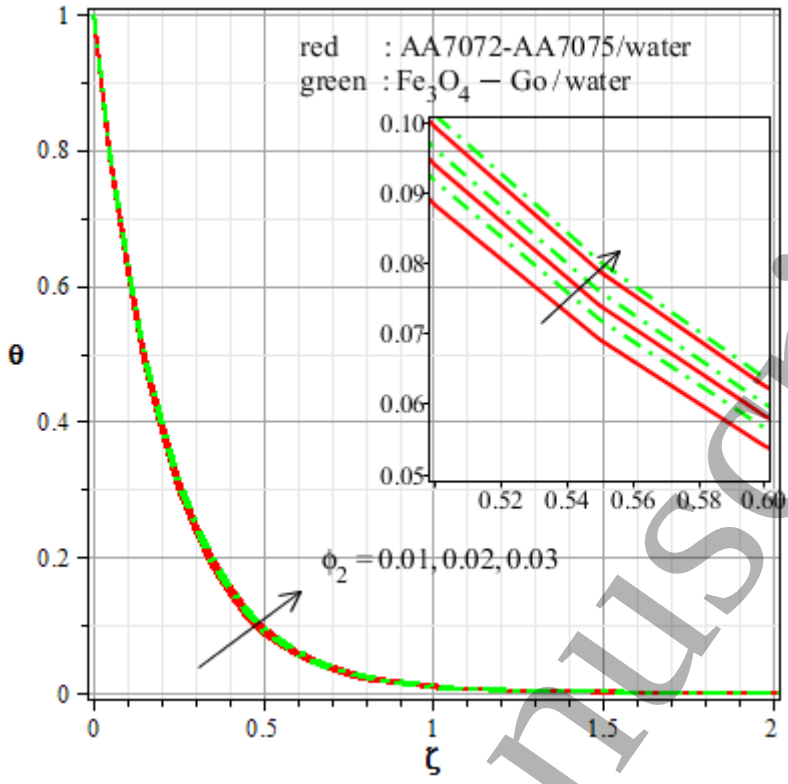

Fig. 12: Temperature curve for different ϕ_2.

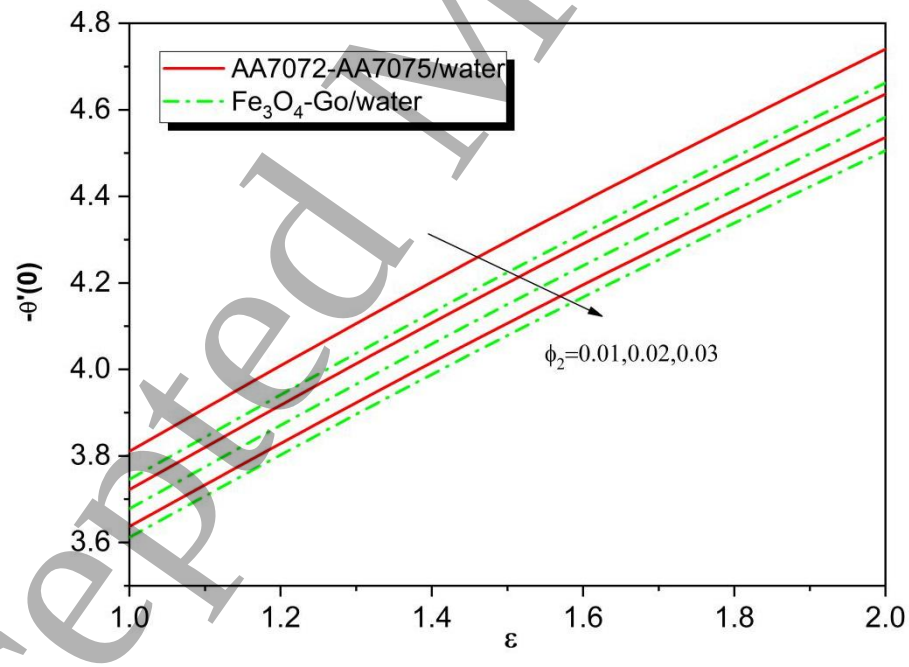

Fig. 13: Nusselt number for different ϕ_2 and ε.

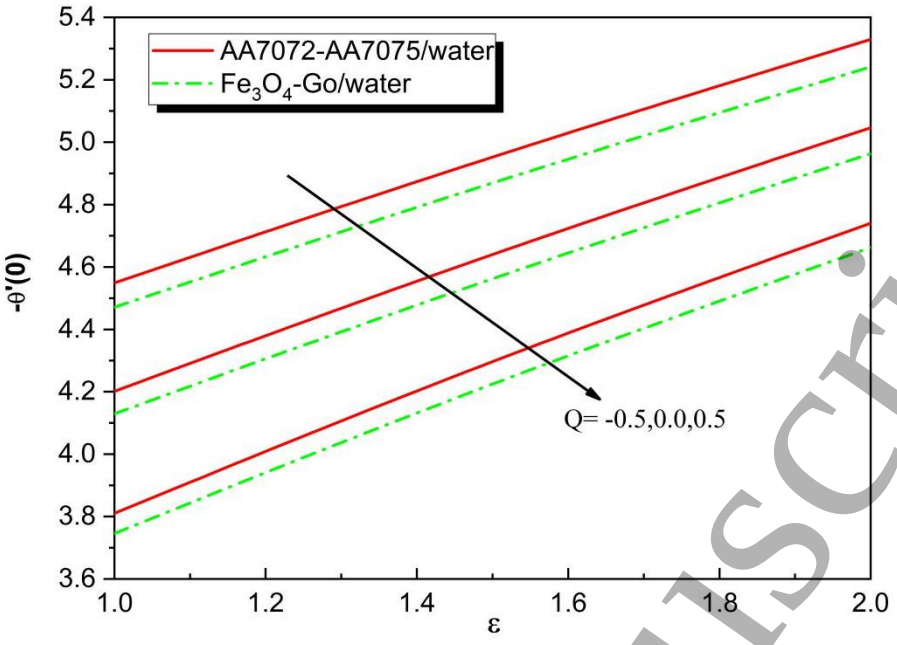

Figure 14: Nusselt number for different Q and ε.

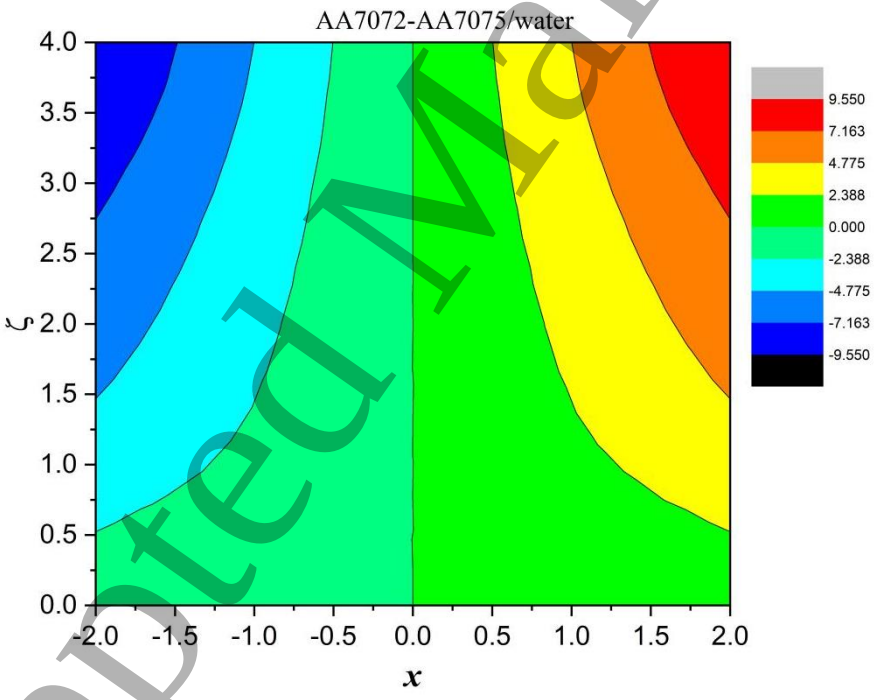

Fig. 15: Streamline pattern for AA7072-AA7075/H_2O.

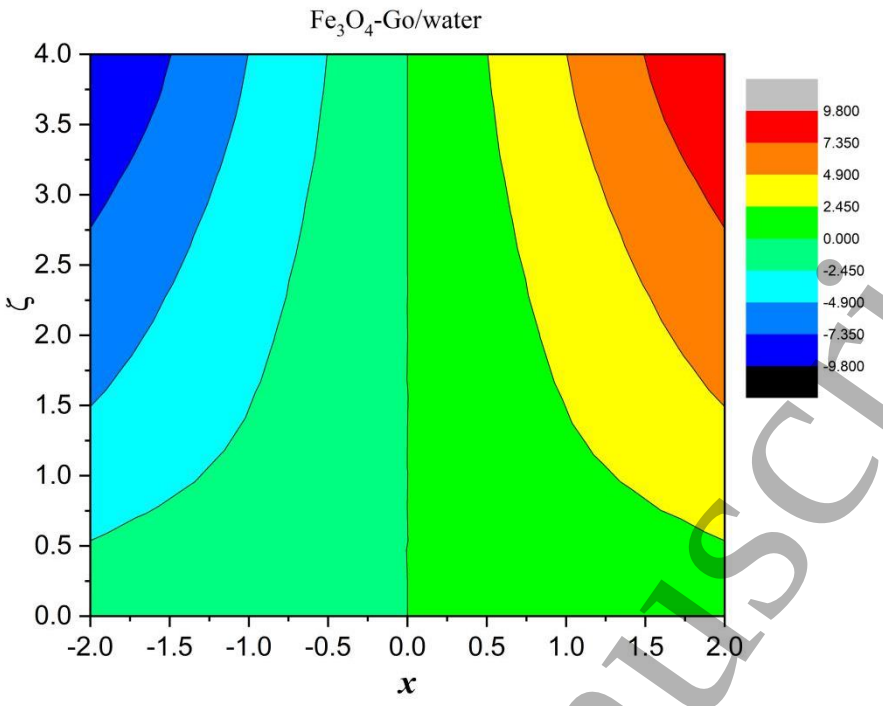

Fig. 16: Streamline pattern for Fe_3O_4-Go/H_2O.